Low Molecular Mass Organogelator Based Gel Electrolyte with Effective Charge Transport Property for Long-Term Stable Quasi-Solid-State Dye-Sensitized Solar Cells

ARTICLE *in* THE JOURNAL OF PHYSICAL CHEMISTRY B · OCTOBER 2008

Impact Factor: 3.3 · DOI: 10.1021/jp8052168 · Source: PubMed

10 AUTHORS, INCLUDING:

Songyuan Dai
North China Electric Power University
216 PUBLICATIONS **2,251** CITATIONS
SEE PROFILE

Fantai Kong
Chinese Academy of Sciences
33 PUBLICATIONS **768** CITATIONS
SEE PROFILE

Xiaqin Fang
Chinese Academy of Sciences
22 PUBLICATIONS **460** CITATIONS
SEE PROFILE

Xu Pan
Chinese Academy of Sciences
49 PUBLICATIONS **1,045** CITATIONS
SEE PROFILE

THE JOURNAL OF PHYSICAL CHEMISTRY B

Article

Low Molecular Mass Organogelator Based Gel Electrolyte with Effective Charge Transport Property for Long-Term Stable Quasi-Solid-State Dye-Sensitized Solar Cells

Zhipeng Huo, Songyuan Dai, Changneng Zhang, Fantai Kong, Xiaqin Fang, Lei Guo, Weiqing Liu, Linhua Hu, Xu Pan, and Kongjia Wang

J. Phys. Chem. B, **2008**, 112 (41), 12927-12933 • DOI: 10.1021/jp8052168 • Publication Date (Web): 18 September 2008

Low Molecular Mass Organogelator Based Gel Electrolyte with Effective Charge Transport Property for Long-Term Stable Quasi-Solid-State Dye-Sensitized Solar Cells

Zhipeng Huo, Songyuan Dai,* Changneng Zhang, Fantai Kong, Xiaqin Fang, Lei Guo, Weiqing Liu, Linhua Hu, Xu Pan, and Kongjia Wang

Division of Solar Energy Materials and Engineering, Institute of Plasma Physics, Chinese Academy of Sciences (ASIPP), Hefei, 230031, P. R. China

Received: June 13, 2008; Revised Manuscript Received: July 30, 2008

Stable quasi-solid-state dye-sensitized solar cells (DSC) were fabricated using 12-hydroxystearic acid as a low molecular mass organogelator (LMOG) to form gel electrolyte. TEM image of the gel exhibited the self-assembled network constructed by the LMOG, which hindered flow and volatilization of the liquid. The formation of less-mobile polyiodide ions such as I_3^- and I_5^- confirmed by Raman spectroscopy increased the conductivity of the gel electrolytes by electronic conduction process, which should be rationalized by the Grotthuss-type electron exchange mechanism caused by rather packed polyiodide species in the electrolytes. The results of the accelerated aging tests showed that the gel electrolyte based dye-sensitized solar cell could retain over 97% of its initial photoelectric conversion efficiency value after successive heating at 60 °C for 1000 h and device degradation was also negligible after one sun light soaking with UV cutoff filter for 1000 h.

1. Introduction

Because of high-efficiency and potential low-cost, dye-sensitized solar cells (DSC), which may be an alternative to conventional inorganic photovoltaic devices,[1] are currently attracting widely to both academic and commercial interests. An impressive photoelectric conversion efficiency greater than 10% has been obtained for photovoltaic devices with organic solvent based electrolytes,[2−8] and our 500 W DSC showcase for outdoor application was founded in 2004, which gives a picture of the prospective industrial application in the near future.[9] However, the presence of liquid electrolytes in such modules may result in some practical limitations of sealing and long-term stability caused by the leakage of the liquid electrolyte. Therefore, p-type semiconductor,[10,11] hole-conductor,[12] and polymeric materials incorporating the redox couple I_3^-/I^-,[13−17] which can be used as solid-state electrolyte, have been attempted to substitute for the liquid electrolyte in DSC. However, the contact between hole transporting materials and the nanoporous semiconductor films is under development, and the photovoltaic performance of solid-state DSC is still too low for practical application.

According to the reports, gelation of organic solvent based or ionic liquid based liquid electrolytes with polymers,[18−20] nanoparticles,[19,21−23] or low molecular mass organogelators (LMOGs)[24,25] can produce quasi-solid-state electrolytes for dye-sensitized solar cells with good photovoltaic performance. The low molecular mass organogelators constitute an important class of functional materials with a broad range of applications in templated material synthesis, drug delivery systems, personal care products, separation technology, and biomimetics.[26−31] The molecules of LMOGs are capable of self-organizing into finely dispersed anisotropic aggregates within the organic solvent to form three-dimensional (3D) structure by very specific and balanced supramolecular interactions of the gelator molecules such as hydrogen bonding, hydrophobic interactions, π-π interactions, and electrostatic interactions. Such network structures commonly melt upon heating but are reformed again during the cooling process, revealing the thermoreversibility of the system. This is an advantage of the LMOGs. Because of the thermoreversibility, above the solution-to-gel transition temperature (T_{SG}), the hot solution of the electrolyte can efficiently fill the nanopores of the nanoporous TiO_2 photoelectrode, and upon cooling, the molecules of LMOGs are self-assembling to form a 3D network in the internal space between the nanoporous TiO_2 photoelectrode and the counter electrode of the DSC; then, a mechanically stable quasi-solid-state electrolyte is obtained. These characteristics triggered our interest to develop LMOG based gel electrolytes for quasi-solid-state dye-sensitized solar cells.

Recently, research on applying LMOG based gel electrolytes to quasi-solid-state DSC, the charge transport mechanism of the electrolytes gelated by LMOGs, and the long-term stability of the corresponding DSC is still very few. In this paper, for the first time, 12-hydroxystearic acid was introduced into 3-methoxypropionitrile (MePN) based liquid electrolyte as a low molecular mass organogelator to form gel electrolyte for quasi-solid-state dye-sensitized solar cells (shown in Figure 1). We report our research results about the gelation ability of this kind of LMOG, the charge transport mechanism of this kind of LMOG based gel electrolyte, the photovoltaic performance, and both the thermostability and photostability of the corresponding quasi-solid-state dye-sensitized solar cells in detail.

2. Experimental Section

2.1. Preparation of Dye-Sensitized Nanoporous TiO_2 Photoelectrode. By screen-printing double layer 25 nm-sized TiO_2 nanoparticles[32] on transport conducting glass (FTO, TEC-8, LOF), a 20 μm thick TiO_2 film was prepared as photoelectrode; then, it was coated with a 3 μm thick 300 nm-sized light-scattering anatase particles. After sintering at 500 °C for 30 min in air and then cooling to about 80 °C, the nanoporous TiO_2 photoelectrode was immersed in an anhydrous ethanol solution with 5×10^{-4} mol/L *cis*-dithiocyanate-*N*,*N*′-bis-(4-

* To whom correspondence should be addressed. Phone: +86-551-5591377 Fax: +86-551-5591377. E-mail: sydai@ipp.ac.cn.

10.1021/jp8052168 CCC: $40.75
Published on Web 09/18/2008

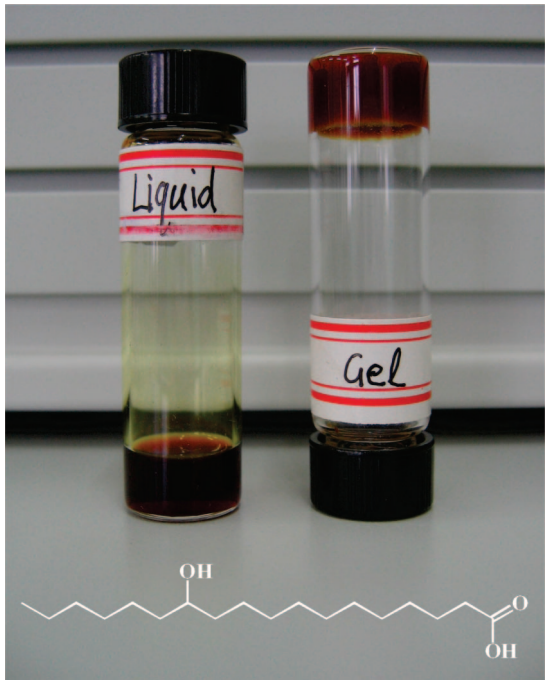

Figure 1. Photo of liquid and low molecular mass organogelator based gel (the bottle is upside down) electrolytes (from left to right).

carboxylate-4-tetrabutylammonium carboxylate-2,2′-bipyridine) ruthenium(II) (N719) for 12 h and then assembled with platinized counter electrode. Two electrodes were separated by hot-melt Surlyn polymer (Surlyn 1702) film and sealed up by heating.

2.2. Preparation of the Electrolytes. 1,2-Dimethyl-3-propylimidazolium iodide (DMPII) was synthesized as reported previously.[33] The composition of liquid electrolyte A is as follows: 0.6 mol/L 1,2-dimethyl-3-propylimidazolium iodide (DMPII), 0.1 mol/L lithium iodide anhydrous (98%, Fluka), 0.1 mol/L iodine, 0.45 mol/L *N*-methyl-benzimidazole (NMBI: 99%, Aldrich) in 3-methoxypropionitrile (MePN: 99%, Fluka). The gel electrolyte B was prepared by adding 5 wt % (vs liquid electrolyte A) 12-hydroxystearic acid (99%, Aldrich) into liquid electrolyte A and heated under stirring until the low molecular mass organogelator melted. After cooling down to room temperature, the gel electrolyte was formed.

2.3. Fabrication of the DSC. By using a vacuum pump, the liquid electrolyte was injected into the internal space of the cell through the hole on the counter electrode, and the hole was sealed by heating the hot-melt Surlyn film (Surlyn 1702) between the thin glass cover and counter electrode. The gel electrolyte was heated to 80 °C under stirring until the gel completely melted. Then, the electrolyte (hot solution) was injected into the internal space of the cell through the hole made on the counter electrode, and the hole was sealed by heating the hot-melt Surlyn film between the thin glass cover and counter electrode. After cooling down to room temperature, a uniform motionless gel layer was formed in cell.

2.4. Electron Microscopic Observation. For the transmission electron microscopy, the gel was dispersed in MePN solvent by sonicating; then, the phosphotungstic acid (PTA) staining electron microscopical technique was used to observe the image of gel network. The transmission electron microscopy measurement was performed with a transmission electron microscope (JEM-100SX, JEOL, Japan).

2.5. Differential Scanning Calorimetry. The solution-to-gel transition temperature (T_{SG}) of the gel electrolyte was determined by using differential scanning calorimeter (DSC821^e/700 METTLER TOLEDO). The measurements were performed with samples of 10−30 mg at a heating rate of 5 °C·min^{-1} under nitrogen in a temperature range of 5−100 °C.

2.6. Voltammetric Measurements. The dark current−voltage characteristic data were obtained by linear sweep voltammetry by using an electrochemical workstation (CHI660A, CH Instruments Inc., Austin, TX). The working electrode was the dye-sensitized TiO_2 film of DSC. The auxiliary electrode and the reference electrode were the platinized conducting glass of DSC. The scan rate was 10 mV/s.

2.7. Conductivity Measurements. Conductivity measurements were carried out using two electrodes thin-layer cells. The cell apparatus for conductivity measurements was equipped as follows: Two platinum black electrodes were fixed by a silicone rubber stopper. The gel electrolyte was heated until the gel was dissolved in a sample vial. The resulting vial was stoppered with silicone rubber stopper equipped with platinum black electrodes. After cooling down to room temperature, the gel electrolyte was formed, then kept at the prescribed temperature for 1.5 h for measuring. The liquid electrolyte was kept in a sample vial. The resulting vial was stoppered with a silicone rubber stopper equipped with platinum black electrodes and then kept at the prescribed temperature for 1.5 h for measuring. The conductivity of the electrolytes was measured by using a frequency response analyzer equipped with a potentiostat (IM6e, Zahner, Germany) at 0 V bias in the frequency range from 50 mHz to 1000 kHz with a modulation amplitude of 5 mV. Conductivity of the electrolytes was determined from the high-frequency intercept with the real axis in the Nyquist plot.[34]

2.8. Electrochemical Impedance Measurements. Impedance measurements were performed with a computer-controlled potentiostat (IM6e, Zahner, Germany) in the frequency range from 20 mHz to 1000 kHz. The magnitude of the alternative signal was 5 mV. The impedance measurements were carried out in dark, and the obtained spectra were fitted with Z-View software in terms of appropriate equivalent circuits.

2.9. Raman Spectroscopy Measurements. The Raman spectra of the electrolytes were recorded on a laser micro-Raman spectrometer (LABRAM-HR, JY., France) equipped with a 514 nm argon laser. The laser spot size was approximately 4−5 μm^2; the power at the sample was estimated to be 1 mW.

2.10. Photoelectrochemical Measurements. The photovoltaic performance of DSC was measured by a Keithley 2420 3A source meter controlled by Testpoint software under solar simulator (Xenon lamp, AM 1.5, 100 mW/cm^2, Changchun Institute of Optics Fine Mechanics and Physics, Chinese Academy of Sciences, calibrated with standard crystalline silicon solar cell). The incident light intensity was calibrated with a standard crystalline silicon solar cell before each experiment. The total covered active electrode area with black mask of DSC was 0.16 cm^2. Hermetically sealed cells were used for long-term stability tests. The cells were stored in the oven at 60 °C for thermal stress. During successive one sun light soaking experiment, the cells covered with UV cutoff filter (up to 394nm) were irradiated at open circuit under a Xenon lamp (XQ3000, 100 mW/cm^2, Shanghai DianGuang Equipment Ltd., China), and the air temperature was set to approximately 50 °C.

3. Results and Discussion

3.1. Gelation Studies of the Low Molecular Mass Organogelator Based Gel. The formation of the supramolecular structures by the organogelator can be investigated using the electron microscopical technique. Figure 2 shows the TEM

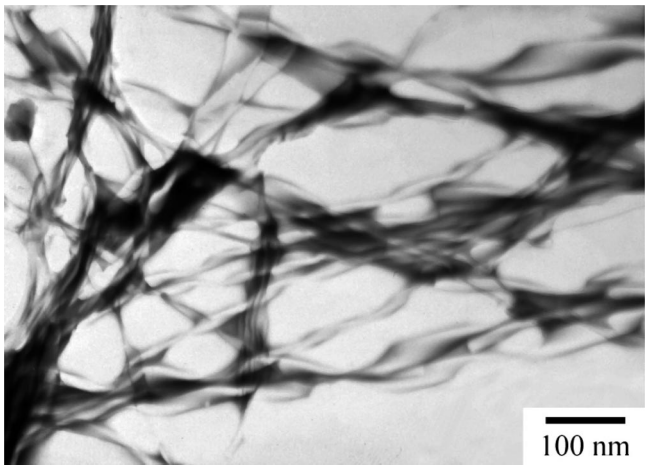

Figure 2. Transmission electron micrographs of low molecular mass organogelator based gel in MePN.

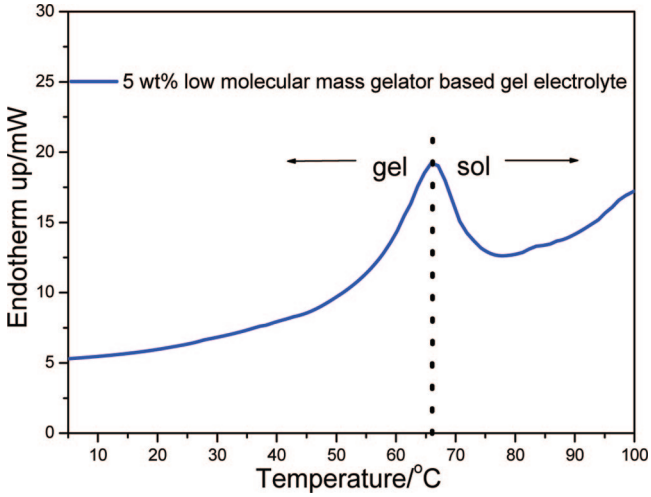

Figure 3. Differential scanning calorimetric thermograms of low molecular mass organogelator based gel.

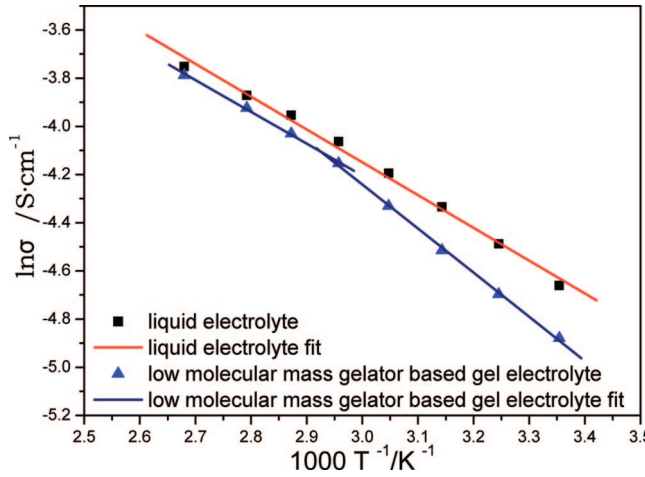

Figure 4. Arrhenius plots for the conductivity of liquid electrolyte and low molecular mass organogelator based gel electrolyte.

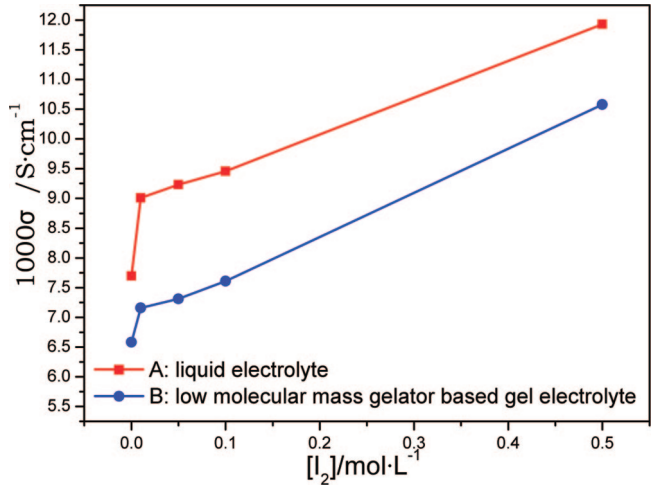

Figure 5. Effect of the concentration of I_2 on conductivity for liquid electrolyte (A) and low molecular mass organogelator based gel electrolyte (B) at 25 °C.

image of the MePN gel formed by the self-assembly of 12-hydroxystearic acid molecules. This image exibited fine fibrillar structures, indicating that the gelator forms a 3D network in MePN liquid.

The thermogram of the gel shows an endothermic signal with its maximum at 66 °C (shown in Figure 3) corresponding to the solution-to-gel transition temperature (T_{SG}). This transition temperature means that below 66 °C the electrolyte maintains a gel state and above this point the network collapses and a liquid is obtained.

After complete dissolution of the organogelator at elevated temperatures, the gelator molecules build up nanoscale fibrils due to the formation of hydrogen bonds and form a 3D network. This leads to gelation of the liquid and hinders flow of the liquid.

3.2. Electrochemical Characteristics of the Gel Electrolyte. We characterized the electrochemical properties of the gel electrolyte in detail. Figure 4 shows the plots of conductivity against $1/T$ for the gel electrolyte and the corresponding liquid electrolyte. The temperature dependence shows a classical Arrhenius behavior obeying the following equation:

$$\sigma = A\exp(-E_A/kT) \quad (1)$$

where σ is the conductivity, A is the pre-exponentional factor, E_A is the activation energy, and k is Boltzmann's constant.

It is shown that the gelation using this kind of low molecular mass organogelator slightly decreased the conductivity when compared to that of the liquid electrolyte in the measured region of the temperature. It is observed that the activation energy value of the gel electrolyte was apparently but slightly changed at around T_{SG} (T_{SG} was 66 °C). Below this transition temperature, the gel electrolyte gave a higher activation energy (15 kJ·mol^{-1}) than that of the corresponding liquid electrolyte (11 kJ·mol^{-1}). But, above this point, the gel electrolyte gave an equal activation energy (11 kJ·mol^{-1}) as that of the corresponding liquid electrolyte. This result suggested that the channel for the charge transport in gel electrolyte could be altered by the self-assembled network constructed by the low molecular mass organogelator. In the electrolytes, the ionic radius of iodide is 2.2 Å, and the covalent radius of iodine is 1.3 Å,[35] but the dimension of the fibril of this kind of gel is nanoscale according to the TEM image of the gel shown in Figure 2. Therefore, the network of this kind of gel could hinder the physical diffusion of the charges in the electrolytes.

3.3. Effect of Polyiodide Species on Conductivity of the Gel Electrolyte. Figure 5 shows the effect of the concentration of I_2 on conductivity for liquid electrolyte and gel electrolyte at 25 °C. When I_2 was introduced into the electrolytes, the conductivity of the electrolytes changed remarkably. As shown in Figure 5, the drastic improvement of the conductivity is clearly proved due to the addition of I_2 in both systems and the increments in conductivity were not linear. With the increase

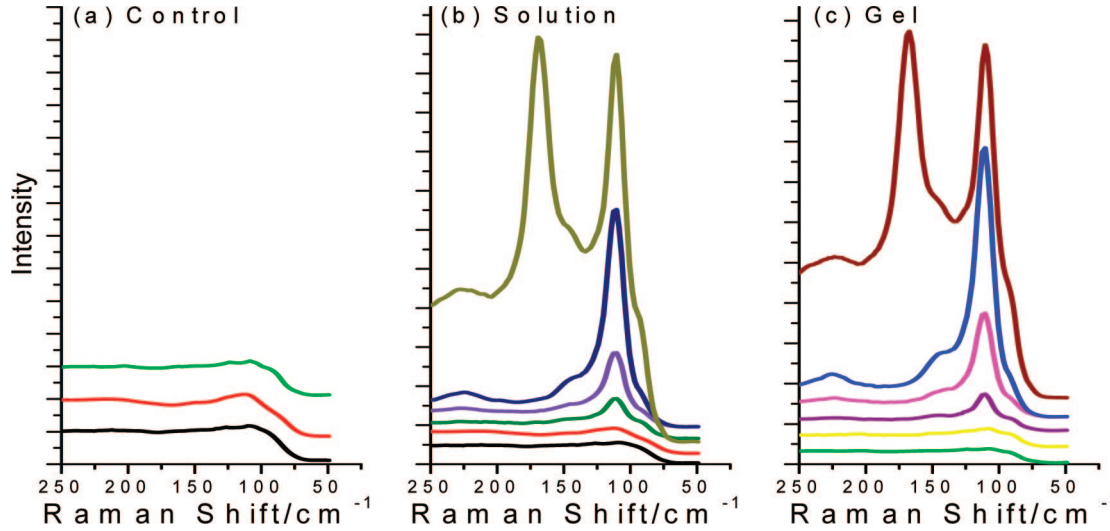

Figure 6. Raman spectra of the electrolytes. (a) Control solutions: MePN (black curve), 0.5 M DMPII in MePN (red curve), and 5 wt % gelator solved in MePN (green curve). (b) Liquid electrolytes: MePN (control: black curve), 0.5 M DMPII with 0 M I_2 (red curve), 0.01 M I_2 (olive curve), 0.05 M I_2 (violet curve), 0.1 M I_2 (navy curve), and 0.5 M I_2 (dark yellow curve) in MePN solvent. (c) Gel electrolytes: 5 wt % gelator in MePN (control: green curve), 0.5 M DMPII with 0 M I_2 (yellow curve), 0.01 M I_2 (purple curve), 0.05 M I_2 (magenta curve), 0.1 M I_2 (blue curve), and 0.5 M I_2 (wine curve).

of the concentration of iodine, the difference of the conductivity between the gel and the liquid electrolyte was being reduced. These results suggest that a special charge transport mechanism should contribute to these phenomena.

Since polyiodides could be formed at the high concentration of I_2 in the presence of iodide ions, polyiodide was thought to contribute to the charge transport process. In order to explain the largely increased conductivity at high concentration of I_2, we examined the formation of polyiodides (I_{2n+1}^-) in the electrolytes. Figure 6 shows Raman spectra of different electrolytes. In Figure 6a, the spectra of MePN solvent, a MePN solution containing 0.5 M DMPII, and a MePN solution containing 5 wt % of gelator are shown as control spectra. The control spectra shows no apparent band in the Raman shift region of 50−250 cm^{-1} except for the broadband around 110 cm^{-1}, which is attributable to the presence of MePN. Figure 6b,c shows the spectra of liquid and gel electrolytes containing 0.5 M of DMPII and I_2; the apparent band was observed around 110 cm^{-1}, which was assigned to the symmetric stretch of I_3^-.[36,37] Interestingly, this band intensity increased with increase of the concentration of I_2; however, it was not observed in the absence of I_2. Moreover, at a higher concentration of I_2, another band around 145 cm^{-1} was observed as a shoulder of the main I_3^- band, and the apparent band was observed around 170 cm^{-1} with a shoulder band around 150 cm^{-1}. These new bands were assigned to the vibration mode of higher polyiodides, such as I_5^-, which have been reported previously.[38] As the Raman spectra show, these bands in gel electrolytes were a little more apparent than those in liquid electrolytes, which may be caused by the packed space in the 3D network of the gel electrolytes.

The conductivity of the electrolyte solution was generally expressed by diffusional ion migration, and polyiodides have relatively lower limiting molar conductivities than the monoiodide due to their large ionic radius.[39] In the electrolytes, the added I_2 was consumed for forming polyiodides. The ionic radius of iodide species increased with the addition of I_2 due to the formation of polyiodide. Consequently, the ionic component in the charge transport process should be unchanged or decreased with an increase in I_2 in the electrolytes. Assuming that the conductivity be only determined by diffusion or migration of ionic species in the electrolytes, the formation of the large polyiodide ions especially in the gel electrolyte should have decreased the conductivity of the electrolyte. As shown in Figure 5, however, the conductivity increased drastically with the concentration of polyiodides.

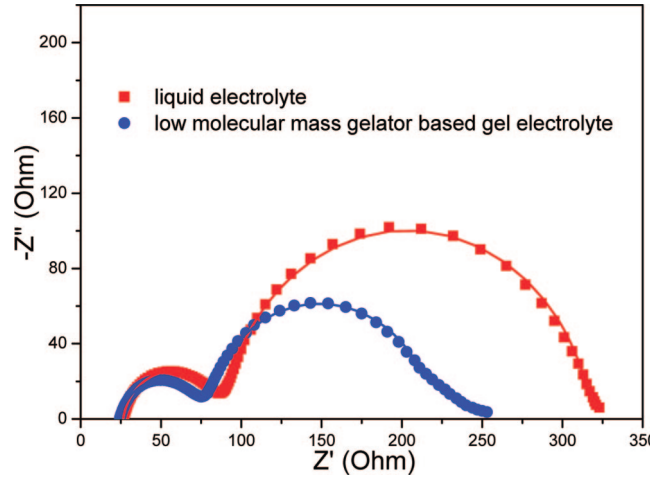

Figure 7. Nyquist plots of liquid electrolyte based cell (A) and the gel electrolyte based cell (B) measured at −0.67 V in the dark. The lines show the fitted results.

Since the redox couple in electrolyte often causes electronic conduction process and the electron exchange between redox couples plays a role in electronic conduction,[40−46] these phenomena could be interpreted as an increased charge exchange mechanism (i.e., Grotthuss mechanism[47]) where electron hopping and the chemical bonds of polyiodides exchange were coupled, which was caused by rather packed polyiodide species in the electrolytes. This mechanism can be described by the Dahms−Ruff equation:[48]

$$D_{app} = D_{phys} + D_{ex} = D_{phys} + k_{ex}\delta^2 c/6 \qquad (2)$$

where D_{phys} is the physical diffusion coefficient, k_{ex} is the electron exchange rate constant, δ is the equilibrium center-to-center distance at the exchange reaction, and c is the total concentration of the redox couple in the electrolyte. The second term in eq 2 (i.e., $k_{ex}\delta^2 c/6$) is the electron exchange diffusion

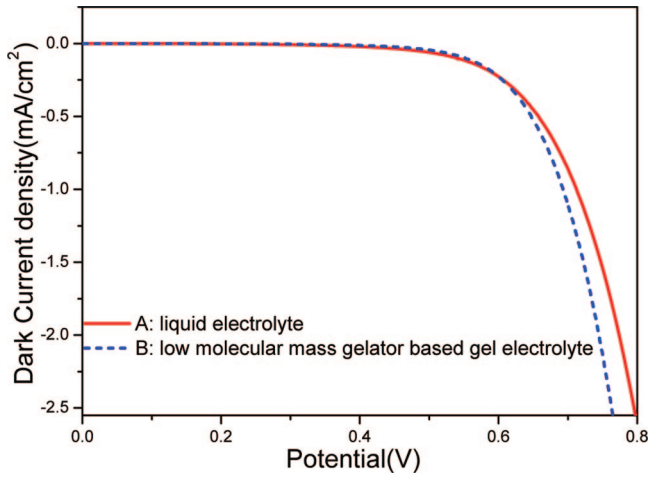

Figure 8. Dark current−voltage characteristics of liquid electrolyte based cell (A) and the gel electrolyte based cell (B) at the scan rate of 10 mV/s.

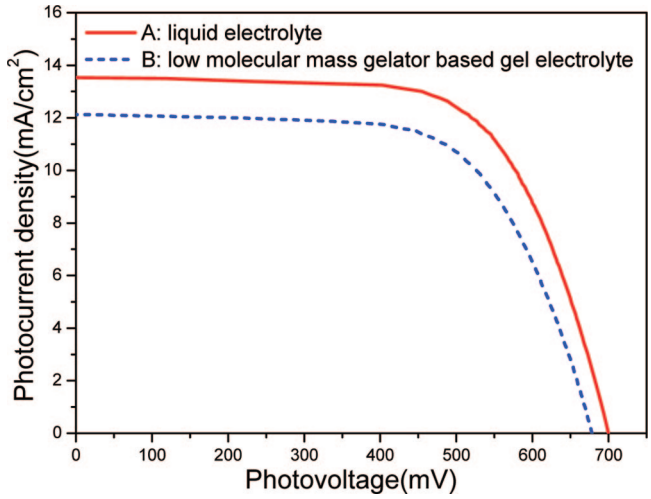

Figure 9. Photocurrent density−voltage characteristics of DSC based on liquid electrolyte (A) and low molecular mass organogelator based gel electrolyte (B) at AM 1.5.

coefficient (D_{ex}). The electron exchange reaction here can be expressed by

$$I^- + I_3^- \xrightarrow{K_{ex}} I_3^- + I^-$$

As Figure 5 shows, the conductivity of the gel electrolytes was only slightly lower than that of the corresponding liquid electrolytes. For instance, the conductivity of the gel electrolyte was 7.61×10^{-3} S·cm^{-1} at 25 °C when the total concentration of I_2 is 0.1 M, which is a little lower than that of the corresponding liquid electrolyte (9.46×10^{-3} S·cm^{-1}). These results indicated that the 3D network of this kind of gel hindered the physical diffusion of the ions in the gel electrolytes, while the electron exchange diffusion caused by the electron exchange reaction reduced this negative effect. This electron exchange mechanism should contribute to the effective charge transport in the gel electrolytes.

3.4. Studies of the Charge Recombination at the Dyed TiO_2 Photoelectrode/Electrolyte Interface. In the dark, the DSC behave as a leaking capacitor.[49] Under forward bias in the dark, electrons are transported through the nanoporous TiO_2 photoelectrode and react with I_3^-. At the same time, I^- is oxidized to I_3^- at the counter electrode. The dark reaction impedance caused by electron transfer from the conduction band of the nanoporous TiO_2 film to triiodide ions in the electrolyte is presented by the semicircle in intermediate frequency regime in the Nyquist plots.[50] The bigger the middle frequency semicircle in the Nyquist plots is, the slighter the electron recombination at the dyed TiO_2 photoelectrode/electrolyte interface is. Figure 7 shows the Nyquist plots of the liquid electrolyte based cell (electrolyte A) and gel electrolyte based cell (electrolyte B) measured at −0.67 V bias in dark. Fitting the middle frequency semicircle gives the chemical capacitance ($C\mu$) and the electron transport resistance (R_{ct}). The fitting result showed that, after gelation by this kind of low molecular mass organogelator, $C\mu$ decreased from 2566 to 2095 μF·cm^{-2} and R_{ct} reduced from 231 Ω to 145 Ω, yielding a shorter electron recombination lifetime (τ) of 76 ms for the gel electrolyte based cell than that for the liquid electrolyte based cell(i.e., 148 ms). The decrease of τ by gelating the electrolyte revealed a much more rapid decrease of the conduction band of the semiconductor than that of the liquid electrolyte based device and an increase of the electron recombination at the dyed TiO_2 photoelectrode/electrolyte interface, which was caused by the conduction band electrons of nanoporous TiO_2 photoelectrode captured by the reduction of I_3^- ions.

Figure 8 shows the dark current−voltage characteristics of the liquid electrolyte and low molecular mass organogelator based gel electrolyte. The dark current−voltage characteristic experiments were performed to investigate the charge recombination at the dyed TiO_2 photoelectrode/electrolyte interface. The results revealed that, after gelation, the dark reaction at the dyed TiO_2 photoelectrode/electrolyte interface was increased.

TABLE 1: Photovoltaic Performance Parameters of Dye-Sensitized Solar Cells Based on the Liquid Electrolyte and Low Molecular Mass Organogelator Based Gel Electrolyte[a]

electrolyte	J_{sc}/mA·cm^{-2}	V_{oc}/V	FF	η/%
A	13.500	0.700	0.663	6.26
B	12.125	0.678	0.652	5.36

[a] Measured at an irradiation of AM 1.5.

3.5. Photovoltaic Performance of Quasi-Solid-State Dye-Sensitized Solar Cell Fabricated Using Low Molecular Mass Organogelator. Figure 9 shows the photocurrent density−voltage characteristics of the liquid electrolyte and gel electrolyte based devices at AM 1.5 (one sun). The photoelectric conversion efficiency (η) and fill factor (FF) were evaluated using the following relations:

$$\eta = \frac{P_m}{P_{in}} = \frac{I_{sc} \times V_{oc} \times FF}{P_{in}} \quad (3)$$

$$FF = \frac{P_m}{I_{sc} \times V_{oc}} = \frac{I_m \times V_m}{I_{sc} \times V_{oc}} \quad (4)$$

where I_{sc} is the short-circuit photocurrent, V_{oc} is the open circuit photo voltage, P_m is the maximum output power, and P_{in} is the incident light power. I_m and V_m represent the maximum current and voltage, respectively. Table 1 summarizes the photovoltaic performance parameters of dye-sensitized solar cells based on liquid electrolyte and low molecular mass organogelator based gel electrolyte at an irradiation of AM 1.5.

These data show that the device based on the low molecular mass organogelator based gel electrolyte (electrolyte B) got a slightly lower photovoltaic performance than the device based on the corresponding liquid electrolyte (electrolyte A). It had smaller short-circuit current density (J_{sc}), open circuit voltage

(V_{oc}), fill factor (FF), and photoelectric conversion efficiency (η) than that based on the corresponding liquid electrolyte.

V_{oc} depends on the dark current that is related to the charge recombination between conduction band electrons and the oxidized half in the electrolyte.[51] The dark reaction is represented by eq 5:

$$I_3^- + 2_{ecb}(TiO_2) \xrightarrow{K_{et}} 3I^- \quad (5)$$

V_{oc} for dye-sensitized solar cells with an iodine redox electrolyte is represented by the following equation:[52]

$$V_{oc} = \frac{kT}{e}\left(\frac{I_{inj}}{n_{cb}k_{et}[I_3^-]}\right) \quad (6)$$

where k and T are the Boltzmann constant and absolute temperature, respectively, I_{inj} is the injection current from dye to semiconductor, n_{cb} is the electron density on the conduction band of semiconductor, and k_{et} represents the rate constant of reduction of I_3^- to I^-. According to eq 6, V_{oc} decreases with an increasing dark reaction. Decrease in V_{oc} of the gel electrolyte based devices could be explained by the enhanced dark reaction. Since the charge transport in the gel electrolyte was slightly hindered by the self-assembled network of the gel, the transportation of I_3^- ions from the dyed TiO_2 photoelectrode/electrolyte interface to the counter electrode was slowed down. Thus, the recombination at the interface between nanoporous TiO_2 photoelectrode and the electrolyte slightly increased; therefore, the dark current slightly increased (shown in Figure 8). As a result, the open circuit voltage (V_{oc}) slightly decreased (from 0.700 to 0.678 V). Moreover, both J_{sc} and FF are influenced by the ionic conductivity of the gel electrolyte, because the decrease in conductivity causes rate-determining of charge transportation and increasing the series resistance.[53] As a result, the short-circuit current density (J_{sc}) (from 13.500 to 12.125 mA·cm^{-2}) and fill factor (FF) (from 0.663 to 0.652) of the DSC slightly decreased. Consequently, compared with the corresponding liquid electrolyte based DSC, photoelectric conversion efficiency (η) (from 6.26 to 5.36%) of the gel electrolyte based DSC decreased.

3.6. Stability of Quasi-Solid-State Dye-Sensitized Solar Cells Fabricated Using Low Molecular Mass Organogelator. Although the device based on the low molecular mass organogelator based gel electrolyte got a slightly lower photovoltaic performance than the device based on the corresponding liquid electrolyte, it exhibited excellent stability. In our experiment, we examined the stability of the devices based on the liquid electrolyte and the low molecular mass organogelator based gel electrolyte both under successive heating and light soaking. Figure 10 shows the comparison of thermostability between the liquid electrolyte based device and gel electrolyte based device at 60 °C thermal stress for 1000 h.

The conversion efficiency of the gel electrolyte based device retained over 97% of its initial value after this period. Figure 11 shows the comparison of stability between the liquid electrolyte based device and gel electrolyte based device during successive one sun light soaking with a UV cutoff filter for 1000 h. The conversion efficiency of the gel electrolyte based device retained 100% of its initial value after this period. These results reveal that the gel electrolyte based device had better stability than the corresponding liquid electrolyte based device. This is because this gel electrolyte had excellent stability and the network of the gel hindered the leakage of the liquid electrolyte effectively.

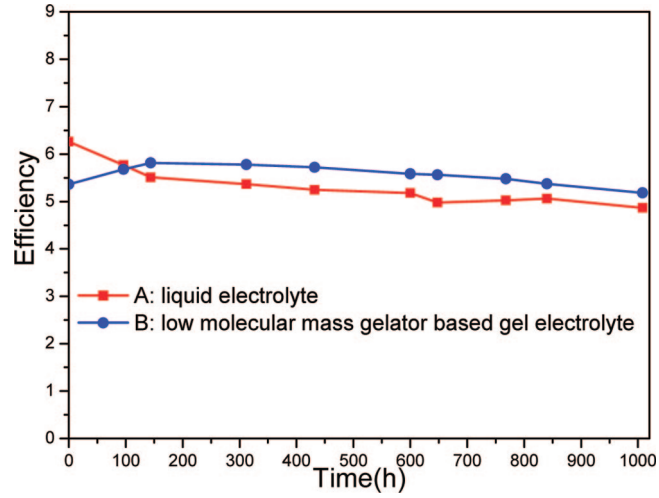

Figure 10. Device efficiency variation with the liquid electrolyte (A) and low molecular mass organogelator based gel electrolyte (B) during accelerated aging tests at 60 °C for 1000 h.

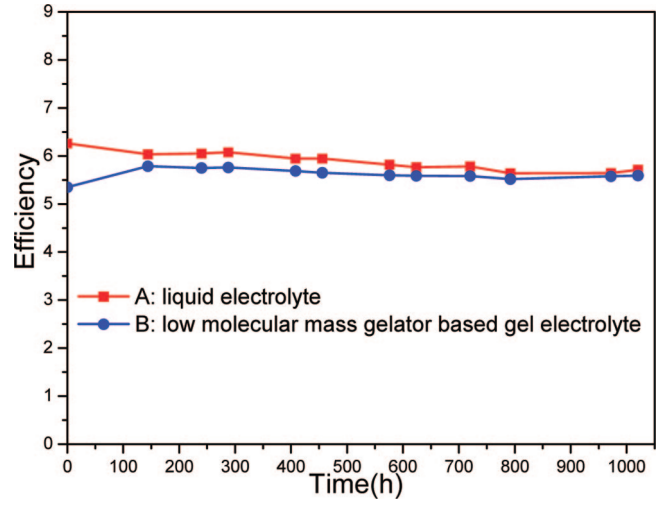

Figure 11. Device efficiency variation with the liquid electrolyte (A) and low molecular mass organogelator based gel electrolyte (B) during successive one sun light soaking with UV cutoff filter at 50 °C for 1000 h.

4. Conclusion

In summary, 12-hydroxystearic acid was successfully introduced into a MePN based liquid electrolyte as a low molecular mass organogelator (LMOG) to form a gel electrolyte for quasi-solid-state dye-sensitized solar cells. The self-assembled network of the gel constructed by the LMOG was confirmed by TEM image. The conductivity dependence on temperature for the gel electrolyte and the corresponding liquid electrolyte shows a classical Arrhenius behavior. Conductivity measurements revealed that the gelation did not significantly influence the charge transport in the electrolytes. The formation of less-mobile polyiodide ions increased the conductivity of the gel electrolytes, which should be rationalized by the Grotthuss-type electron exchange mechanism caused by rather packed polyiodide species in the electrolytes. These results suggested that the 3D network of the gel hindered the physical diffusion of the ions in the gel electrolytes, while the electron exchange diffusion caused by the electron exchange reaction reduced this negative effect. Importantly, although the device based on the low molecular mass organogelator based gel electrolyte got a slightly lower photovoltaic performance than the device based on the corre-

sponding liquid electrolyte, the results of the accelerated aging tests showed that the gel electrolyte based device could retain over 97% of its initial photoelectric conversion efficiency value after heating at 60 °C for 1000 h and the gel electrolyte based device could retain 100% of its initial photoelectric conversion efficiency value after one sun light soaking for 1000 h, which indicates that this kind of gel electrolyte based device had excellent stability. These results reveal that this gel electrolyte was stable and the network of the gel hindered the leakage of the liquid electrolyte effectively, which contribute significantly to the improvement of the long-term stability of dye-sensitized solar cells. They offer us a method to realize the practical use of dye-sensitized solar cells by using a kind of low molecular mass organogelator to form a gel electrolyte for quasi-solid-state dye-sensitized solar cells with high stability and good performance, and it will enable the fabrication of flexible compact, laminated quasi-solid-state devices free of leakage and available in varied geometries.

Acknowledgment. The authors gratefully acknowledge the support of the National Basic Research Program of China (Grant No. 2006CB202600), the Anhui Province Key Technologies R & D Program (Grant No. 06012024A), and the ICSC—World Laboratory (NET-5 Project). We appreciate the cooperation of Dyesol in Australia and Prof. M. Grätzel, EPFL, in Switzerland.

Supporting Information Available: The method to determine conductivity of the electrolytes was explained by using a full impedance plot of electrolyte (Figure S1) with a suitable equivalent circuit (Figure S2). This material is available free of charge via the Internet at http://pubs.acs.org.

References and Notes

(1) Grätzel, M. *Nature* **2001**, *414*, 338.
(2) Nazeeruddin, M. K.; Kay, A.; Rodicio, I.; Humphry-Baker, R.; Müller, E.; Liska, P.; Vlachopoulos, N.; Grätzel, M. *J. Am. Chem. Soc.* **1993**, *115*, 6382.
(3) Nazeeruddin, M. K.; Péchy, P.; Renouard, T.; Zakeeruddin, S. M.; Humphry-Baker, R.; Comte, P.; Liska, P.; Cevey, L.; Costa, E.; Shklover, V.; Spiccia, L.; Deacon, G. B.; Bignozzi, C. A.; Grätzel, M. *J. Am. Chem. Soc.* **2001**, *123*, 1613.
(4) Grätzel, M. *J. Photochem. Photobiol., A* **2004**, *164*, 3.
(5) Wang, Z. S.; Kawauchi, H.; Kashima, T.; Arakawa, H. *Coord. Chem. Rev.* **2004**, *248*, 1381.
(6) Wang, Z. S.; Yanagida, M.; Sayama, K.; Sugihara, H. *Chem. Mater.* **2006**, *18*, 2912.
(7) Wang, Z. S.; Yamaguchi, T.; Sugihara, H.; Arakawa, H. *Langmuir* **2005**, *21*, 4272.
(8) Koide, N.; Islam, A.; Chiba, Y.; Han, L. Y. *J. Photochem. Photobiol., A* **2006**, *182*, 296.
(9) Dai, S. Y.; Wang, K. J.; Weng, J.; Sui, Y. F.; Huang, Y.; Xiao, S. F.; Chen, S. H.; Hu, L. H.; Kong, F. T.; Pan, X.; Shi, C. W.; Guo, L. *Sol. Energy Mater. Sol. Cells* **2005**, *85*, 447.
(10) Zhang, C. N.; Wang, K. J.; Hu, L. H.; Kong, F. T.; Guo, L. *J. Photochem. Photobiol., A* **2007**, *189*, 329.
(11) Kumara, G. R. R. A.; Konno, A.; Senadeera, G. K. R.; Jayaweera, P. V. V.; De Silva, D. B. R. A.; Tennakone, K. *Sol. Energy Mater. Sol. Cells* **2001**, *69*, 195.
(12) Bach, U.; Lupo, D.; Comte, P.; Moser, J. E.; Weissörtel, F.; Salbeck, J.; Spreitzer, H.; Grätzel, M. *Nature* **1998**, *395*, 583.
(13) Cao, F.; Oskam, G.; Searson, P. C. *J. Phys. Chem.* **1995**, *99*, 17071.
(14) Dissanayke, M. A. K. L.; Bandara, L. R. A. K.; Bokalawala, R. S. P.; Jayathilaka, P. A. R. D.; Ileperuma, O. A.; Somasundaram, S. *Mater. Res. Bull.* **2002**, *37*, 867.
(15) Ileperuma, O. A.; Dissanayake, M. A. K. L.; Somasundaram, S. *Electrochim. Acta* **2002**, *47*, 2801.
(16) Wang, P.; Zakeeruddin, S. M.; Exnar, I.; Grätzel, M. *Chem. Commun.* **2002**, 2972.
(17) Asano, T.; Kubo, T.; Nishikitani, Y. *J. Photochem. Photobiol., A* **2004**, *164*, 111.
(18) Guo, L.; Dai, S. Y.; Wang, K. J.; Fang, X. Q.; Shi, C. W.; Pan, X. *Chem. J. Chin. Univ.* **2004**, *26*, 1934.
(19) Wang, P. S.; Zakeeruddin, M.; Grätzel, M. *J. Fluorine Chem.* **2004**, *125*, 1241.
(20) Huo, Z. P.; Dai, S. Y.; Wang, K. J.; Kong, F. T.; Zhang, C. N.; Pan, X.; Fang, X. Q. *Sol. Energy Mater. Sol. Cells* **2007**, *91*, 1959.
(21) Wang, P.; Zakeeruddin, S. M.; Comte, P.; Exnar, I.; Grätzel, M. *J. Am. Chem. Soc.* **2003**, *125*, 1166.
(22) Usui, H.; Matsui, H.; Tanabe, N.; Yanagida, S. *J. Photochem. Photobiol., A* **2004**, *164*, 97.
(23) Yang, H.; Yu, C. Z.; Song, Q. L.; Xia, Y. Y.; Li, F. Y.; Chen, Z. G.; Li, X. H.; Yi, T.; Huang, C. H. *Chem. Mater.* **2006**, *18*, 5173.
(24) Mohmeyer, N.; Wang, P.; Schmidt, H.-W.; Zakeeruddin, S. M.; Grätzel, M. *J. Mater. Chem.* **2004**, *14*, 1905.
(25) Mohmeyer, N.; Kuang, D. B.; Wang, P.; Schmidt, H.-W.; Zakeeruddin, S. M.; Grätzel, M. *J. Mater. Chem.* **2006**, *16*, 2978.
(26) Rees, G. D.; Robinson, B. H. *Adv. Mater.* **1993**, *5*, 608.
(27) Haering, G.; Luisi, P. L. *J. Phys. Chem.* **1986**, *90*, 5892.
(28) Phillips, R. J.; Deen, W. M.; Brady, F. J. *J. Colloid Interface Sci.* **1990**, *139*, 363.
(29) Hafkamp, R. J. H.; Kokke, P. A.; Geurts, H. P. M.; Rowan, A. E.; Feiters, M. C.; Nolte, R. J. M.; Danke, I. M. *Chem. Commun.* **1997**, 545.
(30) Schamper, T.; Jablon, M.; Randhawa, M. H.; Senatore, A.; Warren, J. D. *J. Soc. Cosmet. Chem.* **1986**, *37*, 225.
(31) Beginn, U.; Tartsch, B. *Chem. Commun.* **2001**, 1924.
(32) Hu, L. H.; Dai, S. Y.; Weng, J.; Xiao, S. F.; Sui, Y. F.; Huang, Y.; Chen, S. H.; Kong, F. T.; Pan, X.; Liang, L. Y.; Wang, K. J. *J. Phys. Chem. B* **2007**, *111*, 358.
(33) Shi, C. W.; Dai, S. Y.; Wang, K. J.; Pan, X.; Zeng, L. Y.; Hu, L. H.; Kong, F. T.; Guo, L. *Electrochim. Acta* **2005**, *50*, 2597.
(34) Wang, H. X.; Bell, J.; Desilvestro, J.; Bertoz, M.; Evans, G. *J. Phys. Chem. C* **2007**, *111*, 15125.
(35) Lide, D. R. *Handbook of Chemistry and Physics*, 75th ed.; CRC Press Inc.: Boca Raton, FL, 1994.
(36) Tadayyoni, M. A.; Gao, P.; Weaver, M. J. *J. Electroanal. Chem.* **1986**, *198*, 125.
(37) Andrews, L.; Prochaska, E. S.; Loewenschuss, A. *Inorg. Chem.* **1980**, *19*, 463.
(38) Loos, K. R.; Jones, A. C. *J. Phys. Chem.* **1974**, *78*, 2306.
(39) Popov, A. I.; Rygg, R. H.; Skelly, N. E. *J. Am. Chem. Soc.* **1956**, *78*, 5740.
(40) Dahms, H. *J. Phys. Chem.* **1968**, *72*, 362.
(41) Ruff, I.; Friedrich, V. J. *J. Phys. Chem.* **1971**, *75*, 3297.
(42) Ruff, I.; Friedrich, V. J.; Demeter, K.; Csaillag, K. *J. Phys. Chem.* **1971**, *75*, 3303.
(43) Ruff, I.; Korosi-odor, I. *Inorg. Chem.* **1970**, *9*, 186.
(44) Ruff, I. *Electrochim. Acta* **1970**, *15*, 1059.
(45) Botar, L.; Ruff, I. *Chem. Phys. Lett.* **1986**, *126*, 348.
(46) Botar, L.; Ruff, I. J. *Chem. Phys.* **1985**, *83*, 1292.
(47) Papageorgiou, N.; Athanassov, Y.; Armand, M.; Bonhote, P.; Pettersson, H.; Azam, A.; Grätzel, M. *J. Electrochem. Soc.* **1996**, *143*, 3099.
(48) Kawano, R.; Watanabe, M. *Chem. Commun.* **2003**, 330.
(49) Bisquert, J. *J. Phys. Chem. B* **2002**, *106*, 325.
(50) Wang, Q.; Moser, J.; Grätzel, M. *J. Phys. Chem. B* **2005**, *109*, 14945.
(51) Gregg, B. A.; Pichot, F.; Ferrere, S.; Fields, C. L. *J. Phys. Chem. B* **2001**, *105*, 1422.
(52) Hagfeldt, A.; Grätzel, M. *Chem. Rev.* **1995**, *95*, 49.
(53) Komiya, R.; Han, L. Y.; Yamanaka, R.; Islam, A.; Mitate, T. *J. Photochem. Photobiol., A* **2004**, *164*, 123.

JP8052168